Design of the Telescopic OTA

For a Generic 180nm Bulk CMOS Process (Version 2)

Christian Enz (christian.enz@epfl.ch)

2025-07-25

Table of contents

1 Introduction

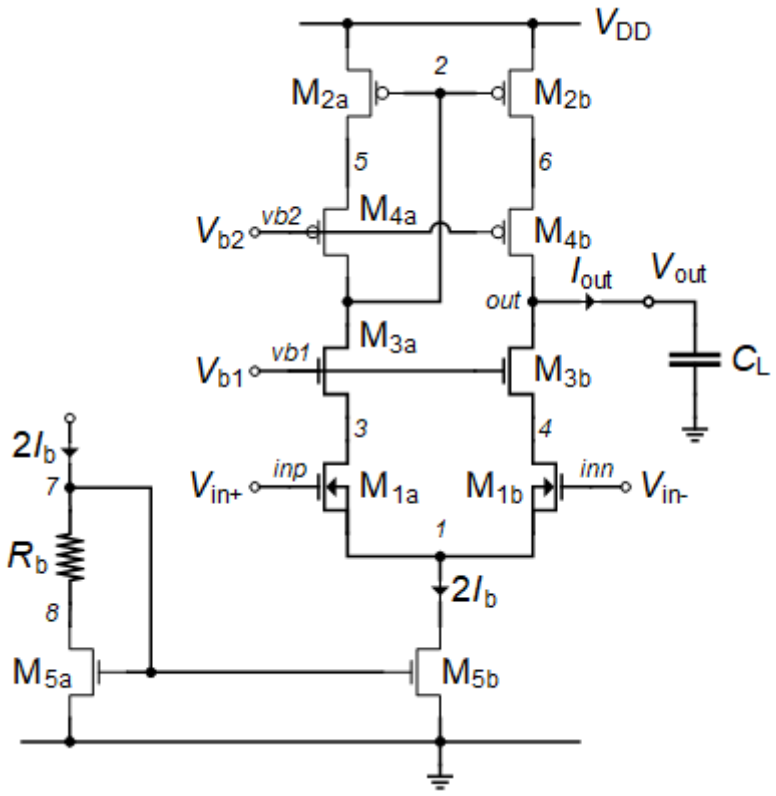

Figure 1.1: Schematic of the telescopic differential OTA.

> **Note**
>
> Note that all nMOS transistors in Figure 1.1 have an odd number and all the pMOS transistors an even number which explains the numbering process.

This notebook presents the analysis, design and simulation of the telescopic cascode OTA which schematic is presented in Figure 1.1 [1]. The design phase is using the sEKV model and the inversion coefficient approach [2], [3], [4]. The telescopic OTA is similar to the simple OTA except that four cascode transistors, namely M_{3a}-M_{3b} and M_{4a}-M_{4b}, have been added to decrease the output conductance and hence increase the DC gain. The GBW and hence the power consumption however remain almost unchanged.

Because of the stacked transistors, this OTA is a bit tricky to design particularly at low-voltage and presents a reduced output voltage swing. In order to save some voltage, we have put M_{1a}-M_{1b} in a separate well. This makes $V_{SB1a} = V_{SB1b} = 0$ and reduces V_{GS1a} and V_{GS1b} to a minimum. When designing the circuit, we particularly need to be careful when sizing the cascode transistors in weak inversion avoiding taking minimum length which would degrade their output conductance and hence the DC gain. This is explained in more details below.

As suggested in [1], we also have added the resistance R_b that will be sized in order for M_{5a} and M_{5b} to have about the same V_{DS} voltage. This makes sure that the current through M_{5a} and M_{5b} are about equal, despite the effect of the output conductance.

We will start with a detailed analysis of the OTA which will allow to derive all the design equations that will be used in the design phase. The OTA is then designed for a given set of specifications for a generic 180 nm bulk CMOS technology. The design is then validated by simulations with ngspice [5] using the EKV 2.6 compact model [6] [7] [8] with parameters corresponding to a generic 180 nm bulk CMOS technology [9] [10].

We now start with the small-signal analysis.

2 Analysis

2.1 Small-signal analysis

We start with the small-signal analysis. The small-signal schematic of the telescopic OTA is shown in Figure 2.1. The analysis of the telescopic OTA is similar to the simple OTA, except that there are now additional nodes due to the cascode transistors.

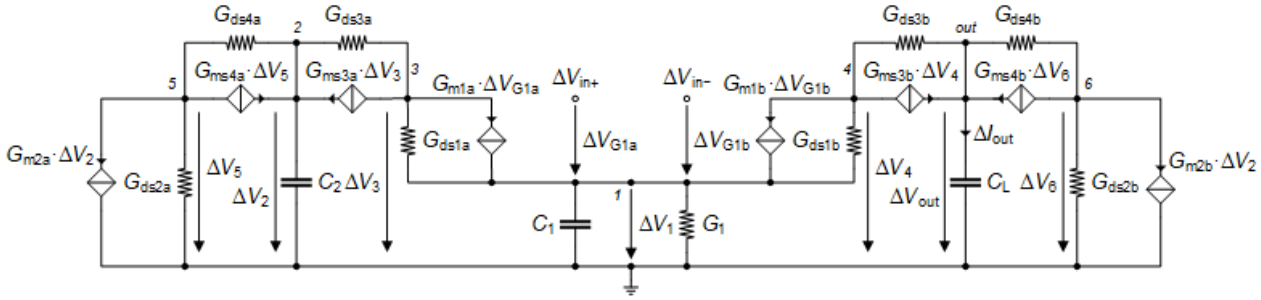

Figure 2.1: Small-signal schematic of the telescopic OTA.

For a differential input voltage, assuming a perfect matching between the transistors in the left and right current branches, the common-source node 1 of the differential pair M_{1a}-M_{1b} remains zero and the small-signal schematic of Figure 2.1 simplifies to the schematic shown in Figure 2.2.

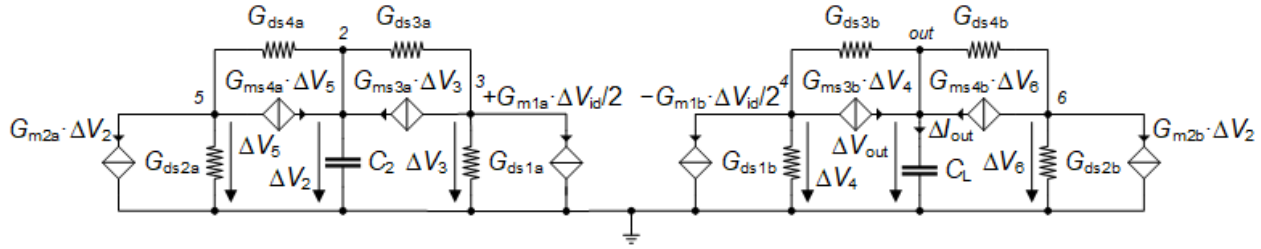

Figure 2.2: Simplified small-signal schematic of the telescopic OTA.

In a 1st-order analysis, we can neglect the capacitances at the low impedance cascode nodes 3, 4, 5 and 6 and only account for the capacitances at high impedance nodes 2 and out. The circuit becomes similar to that of the simple OTA, with the dominant pole ω_0 at the output node (out) and the non-dominant pole ω_p at the current mirror node 2. The transfer function also has a pole-zero doublet. Its transfer function is then given by

$$A_{dm}(s) \triangleq \frac{\Delta V_{out}}{\Delta V_{in}} \cong A_{dc} \cdot \frac{1 + s/\omega_z}{(1 + s/\omega_0)(1 + s/\omega_p)} \cong \frac{A_{dc}}{1 + s/\omega_0} \cong \frac{\omega_u}{s}, \tag{2.1}$$

where

$$A_{dc} \cong \frac{G_{m1}}{G_o}, \tag{2.2}$$

$$G_o \cong \frac{G_{ds1}\, G_{ds3}}{G_{ms3}} + \frac{G_{ds2}\, G_{ds4}}{G_{ms4}}, \tag{2.3}$$

$$\omega_0 \cong \frac{G_o}{C_L}, \tag{2.4}$$

$$\omega_p \cong \frac{G_{m2}}{C_2}, \tag{2.5}$$

$$\omega_z = 2\,\omega_p, \tag{2.6}$$

$$\omega_u = A_{dc} \cdot \omega_0 \cong \frac{G_{m1}}{C_L}. \tag{2.7}$$

We now anlyze the OTA noise in the next section.

2.2 Noise Analysis

At low-frequency the noise of the cascode transistors M_{3a}-M_{3b} and M_{4a}-M_{4b} can be neglected and the noise analysis is then identical to that of the simple OTA. The PSD of the output noise current is given by

$$S_{nout} \cong 2\,(S_{I_{n1}} + S_{I_{n2}}) \tag{2.8}$$

which can be expressed in terms of the output noise conductance as

$$S_{nout} = 4kT \cdot G_{nout}, \tag{2.9}$$

where

$$G_{nout} \cong 2\,(G_{n1} + G_{n2}), \tag{2.10}$$

with

$$G_{ni} = \gamma_{ni} \cdot G_{mi} + G_{mi}^2 \cdot \frac{\rho_i}{W_i\, L_i\, f} \quad \text{for } i = 1, 2. \tag{2.11}$$

The input-referred noise resistance is then given by

$$R_{nin} \triangleq \frac{G_{nout}}{G_{m1}^2} = \frac{2\,(G_{n1} + G_{n2})}{G_{m1}^2} = \frac{2\,G_{n1}}{G_{m1}^2} \cdot \left(1 + \frac{G_{n2}}{G_{n1}}\right) \tag{2.12}$$

which we rewrite as

$$R_{nin} = \frac{2\,G_{n1}}{G_{m1}^2} \cdot (1 + \eta) \tag{2.13}$$

with

$$\eta = \frac{G_{n2}}{G_{n1}}. \tag{2.14}$$

η represents the contribution of the current mirror referred to the input and normalized to the contribution of the differential pair. Of course during the design phase we will try to minimize η.

2.2.1 Input-referred thermal noise

The input-referred thermal noise resistance is given by

$$R_{nth} = \frac{2\,\gamma_{n1}}{G_{m1}} \cdot (1 + \eta_{th}), \tag{2.15}$$

where

$$\eta_{th} = \frac{\gamma_{n2}}{\gamma_{n1}} \cdot \frac{G_{m2}}{G_{m1}} \tag{2.16}$$

represents the contribution to the input-referred thermal noise of the current mirror M_{2a}-M_{2b} relative to that of the differential pair M_{1a}-M_{1b}. In case $G_{m1} \gg G_{m2}$ then $\eta_{th} \ll 1$ and the thermal noise is dominated by the input differential pair. Eqn. (2.16) can then be simplified to

$$R_{nth} \cong \frac{2\,\gamma_{n1}}{G_{m1}}. \tag{2.17}$$

The OTA thermal noise excess factor is then given by

$$\gamma_{ota} \triangleq G_m \cdot R_{nth} \tag{2.18}$$

with $G_m = G_{m1}$ is the OTA equivalent tranbsconductance. The OTA thermal noise excess factor then writes

$$\gamma_{ota} = 2\,\gamma_{n1} \cdot (1 + \eta_{th}). \tag{2.19}$$

In the case $G_{m1} \gg G_{m2}$ then $\eta_{th} \ll 1$ and the noise is dominated by the input differential pair M_{1a}-M_{1b}. The OTA thermal noise excess factor can then be simplified as

$$\gamma_{ota} \cong 2\,\gamma_{n1}. \tag{2.20}$$

2.2.2 Input-referred flicker noise

The input-referred flicker noise is given by

$$R_{nfl} = \frac{2}{f}\ \left[\frac{\rho_n}{W_1\,L_1} + \left(\frac{G_{m2}}{G_{m1}}\right)^2\ \frac{\rho_p}{W_2\,L_2}\right] \tag{2.21}$$

which can be rewritten as

$$R_{nfl} = \frac{2\rho_n}{W_1\,L_1\,f} \cdot (1 + \eta_{fl}) \tag{2.22}$$

where

$$\eta_{fl} = \frac{\rho_p}{\rho_n}\ \left(\frac{G_{m2}}{G_{m1}}\right)^2\ \frac{W_1\,L_1}{W_2\,L_2} \tag{2.23}$$

represents the contribution to the input-referred flicker noise of the current mirror M_{2a}-M_{2b} relative to that of the differential pair M_{1a}-M_{1b}. If M_{1a}-M_{1b} and M_{2a}-M_{2b} have about the same gate area, then η_{fl} can be made small by making $G_{m1} \gg G_{m2}$.

The corner frequency is the frequency at which the flicker noise becomes equal to the thermal noise

$$R_{nfl}(f = f_k) = R_{nth} \tag{2.24}$$

which is given by

$$f_k = \frac{1}{R_{nth}} \cdot \frac{2\rho_n}{W_1\,L_1} \cdot (1 + \eta_{fl}) = \frac{G_{m1}\,\rho_n}{\gamma_{n1}\,W_1\,L_1} \cdot \frac{1 + \eta_{fl}}{1 + \eta_{th}}. \tag{2.25}$$

The transconductance G_{m1} is set by the constraints either on thermal noise or on bandwidth (GBW product). The corner frequency f_k can be reduced by increasing $W_1\,L_1$ and $W_2\,L_2$ at the same time to conserve the same η_{fl} factor. Assuming that $G_{m2}/G_{m1} \ll 1$, as required by the constraints on minimizing the contribution of the current mirror to the input-referred offset and thermal noise, then $\eta_{th} \ll 1$ and $\eta_{fl} \ll 1$ and the corner frequency f_k is then mainly set by the differential pair transconductance and gate transistor area

$$f_k \cong \frac{G_{m1}\,\rho_n}{\gamma_{n1}\,W_1\,L_1}. \tag{2.26}$$

2.3 Input-referred offset voltage

The offset analysis is identical to that of the simple OTA because the contribution of the mismatch of the cascode transistors can be neglected. The random offset current is then mainly due to the mismatch between M_{1a} and M_{1b} and between M_{2a} and M_{2b}. The variance of the output offset current is then given by

$$\sigma^2_{I_{os}} \cong \sigma^2_{\Delta I_{D1}} + \sigma^2_{\Delta I_{D2}} = I_b^2 \cdot \left(\sigma^2_{\frac{\Delta I_{D1}}{I_{D1}}} + \sigma^2_{\frac{\Delta I_{D2}}{I_{D2}}} \right), \tag{2.27}$$

with

$$\sigma^2_{\frac{\Delta I_{Di}}{I_{Di}}} = \sigma^2_{\beta_i} + \left(\frac{G_{mi}}{I_b} \right)^2 \sigma^2_{V_{Ti}} \quad \text{for } i = 1, 2, \tag{2.28}$$

where

$$\sigma^2_{\beta_i} = \frac{A^2_\beta}{W_i\, L_i} \quad \text{for } i = 1, 2 \tag{2.29}$$

is the β-mismatch and

$$\sigma^2_{V_{Ti}} = \frac{A^2_{V_T}}{W_i\, L_i} \tag{2.30}$$

is the V_T-mismatch.

The variance of the output offset current then becomes

$$\sigma^2_{I_{os}} = I_b^2 \cdot (\sigma^2_{\beta_1} + \sigma^2_{\beta_2}) + G^2_{m1} \cdot \sigma^2_{V_{T1}} + G^2_{m2} \cdot \sigma^2_{V_{T2}}. \tag{2.31}$$

The variance of the input-referred offset voltage is obtained by dividing the variance of the output offset current by G^2_{m1} resulting in

$$\sigma^2_{V_{os}} = \left(\frac{I_b}{G_{m1}} \right)^2 (\sigma^2_{\beta_1} + \sigma^2_{\beta_2}) + \sigma^2_{V_{T1}} + \left(\frac{G_{m2}}{G_{m1}} \right)^2 \sigma^2_{V_{T2}} \tag{2.32}$$

which can be written as

$$\sigma^2_{V_{os}} = \sigma^2_{V_{T1}} \cdot (1 + \xi_{V_T}) + \left(\frac{I_b}{G_{m1}} \right)^2 \cdot \sigma^2_{\beta_1} \cdot (1 + \xi_\beta), \tag{2.33}$$

where ξ_{V_T} represents the V_T-mismatch contribution to the input-referred offset of the current mirror relative to that of the differential pair

$$\xi_{V_T} = \left(\frac{G_{m2}}{G_{m1}} \right)^2 \cdot \frac{\sigma^2_{V_{T2}}}{\sigma^2_{V_{T1}}} \tag{2.34}$$

and ξ_β represents the β-mismatch contributions to the input-referred offset of the current mirror relative to that of the differential pair

$$\xi_\beta = \frac{\sigma^2_{\beta_2}}{\sigma^2_{\beta_2}} \tag{2.35}$$

with

$$\sigma_{V_{T1}} = \frac{A^2_{V_{Tn}}}{W_1\, L_1}, \tag{2.36}$$

$$\sigma_{V_{T2}} = \frac{A^2_{V_{Tp}}}{W_2\, L_2} \tag{2.37}$$

and

$$\sigma^2_{\beta_1} = \frac{A^2_{\beta_n}}{W_1\, L_1}, \tag{2.38}$$

$$\sigma^2_{\beta_2} = \frac{A^2_{\beta_p}}{W_2\, L_2}. \tag{2.39}$$

Replacing in (2.34) and (2.35) results in

$$\xi_{V_T} = \left(\frac{G_{m2}}{G_{m1}}\right)^2 \cdot \left(\frac{A_{V_{T_p}}}{A_{V_{T_p}}}\right)^2 \cdot \frac{W_1\, L_1}{W_2\, L_2} \tag{2.40}$$

and

$$\xi_\beta = \left(\frac{A_{\beta_p}}{A_{\beta_n}}\right)^2 \cdot \frac{W_1\, L_1}{W_2\, L_2}. \tag{2.41}$$

Assuming that the V_T-mismatch parameters $A_{V_{Tn}}$ and $A_{V_{Tp}}$ and the area $W_1\, L_1$ and $W_2\, L_2$ are of the same order of magnitude, the contribution of the current mirror M_{2a}-M_{2b} to the V_T-mismatch represented by the ξ_{V_T} parameter can be made small by choosing $G_{m1} \gg G_{m2}$. If this does not suffice, we can increase the area of M_{2a}-M_{2b} keeping its W/L ratio.

The contribution of M_{2a}-M_{2b} to the β-mismatch, represented by the ξ_β factor, is not weighted by the G_m ratio. Assuming that the β-mismatch parameters A_{β_n} and A_{β_p} are of the same order of magnitude, ξ_β can be reduced by increasing the area of M_{2a}-M_{2b} keeping its W/L ratio.

3 Design

3.1 Specifications

The OTA specifications are given in Table 3.1.

> **Note**
>
> The specifications given in Table 3.1 are simplified specifications. They are mainly targeting the achievement of a certain gain-bandwidth product GBW and DC gain at lowest current consumption. The GBW sets the differential pair transconductance while the DC gain sets the output conductance. There is an additional specification on the random input-referred offset voltage which, if not met, might eventually require to increase the transistors area. There are no specifications on thermal noise since the transconductance is set by the GBW. There are no specifications on the flicker noise but if the corner frequency was set lower this would required to increase the transistors area. There are also no specifications on the slew-rate, which might be small because of the low-power objective. Finally, there are many more specifications such as CMRR, PSRR, input common-mode voltage range, output-voltage swing, etc... that are not discussed in this example.

Table 3.1: OTA specifications.

Specification	Symbol	Value	Unit
Minimum DC gain	A_{dc}	100	dB
Minimum gain-bandwidth product	GBW	1	MHz
Load capacitance	C_L	1	pF
Maximum input-referred random offset voltage	V_{os}	10	mV
Phase margin	PM	60	$^\circ$
Corner frequency	f_k	100	kHz

3.2 Process

We will design the cascode gain stage for a generic 180nm bulk CMOS process. The physical parameters are given in Table 3.2, the global process parameters in Table 3.3 and finally the MOSFET parameters in Table 3.4.

Table 3.2: Physical parameters

Parameter	Value	Unit
T	300	K
U_T	25.875	mV

Table 3.3: Global process parameters

Parameter	Value	Unit
V_{DD}	1.8	V
C_{ox}	8.443	$\frac{fF}{\mu m^2}$
W_{min}	200	nm
L_{min}	180	nm

Table 3.4: Transistor process parameters

Parameter	NMOS	PMOS	Unit
sEKV parameters			
n	1.27	1.31	-
$I_{spec\square}$	715	715	nA
V_{T0}	0.455	0.445	V
L_{sat}	26	36	nm
λ	20	20	$\frac{V}{\mu m}$
Overlap capacitances parameters			
C_{GDo}	0.366	0.329	$\frac{fF}{\mu m}$
C_{GSo}	0.366	0.329	$\frac{fF}{\mu m}$
C_{GBo}	0	0	$\frac{fF}{\mu m}$
Junction capacitances parameters			
C_J	1	1.121	$\frac{fF}{\mu m^2}$
C_{JSW}	0.2	0.248	$\frac{fF}{\mu m}$
Flicker noise parameters			
K_F	8.1e-24	8.1e-24	J
AF	1	1	-
ρ	0.05794	0.4828	$\frac{V \cdot m^2}{A \cdot s}$
Matching parameters			
A_{VT}	5	5	$mV \cdot \mu m$
A_β	1	1	$\% \cdot \mu m$
Source and drain sheet resistance parameter			
R_{sh}	600	2386	$\frac{\Omega}{\mu m}$
Width and length parameters			
ΔW	39	54	nm
ΔL	-76	-72	nm

3.3 Design procedure

> **!** Important
>
> For this process, the transistor dimensions are rounded to 10nm. We also will ignore the length and width reduction parameters DL and DW. The main reason is that most of the transistor length and width are sufficiently large that ignoring these parameters has little impact.

3.4 Sizing of M_{1a}-M_{1b}

M_{1a}-M_{1b} are biased in weak inversion in order to minimize the input-referred offset. They are sized according to the specification on the GBW and the load capacitance and the required slew-rate.

Recalling that

$$GBW = \frac{G_{m1}}{2\pi C_{out}}, \tag{3.1}$$

where C_{out} is the total output capacitance which includes the parasitic capacitance and the load capacitance C_L. Since we do not yet know the sizes of M_{1a} and M_{2b}, we cannot estimate the total output capacitance. We will start assuming $C_{out} = C_L$.

G_{m1} is the gate transconductance of M_{1a} and M_{1b} which in deep weak inversion is given by

$$G_{m1} = \frac{I_b}{nU_T}. \tag{3.2}$$

The bias current I_b is the current flowing in each transistor M_{1a} and M_{1b} when the input differential voltage is zero. The bias current provided by M_{3b} is therefore $2I_b$. The bias current must satisfy the following inequality

$$I_b \geq 2\pi\, n_{0n}\, U_T\, C_L\, GBW_{min}. \tag{3.3}$$

which for the given specifications gives $I_{b,min} = 207\ nA$. The corresponding slew-rate is given by $SR_{min} = 207\ mV/\mu s$, which we will consider as sufficient.

> **!** Important
>
> If the slew-rate is not sufficient, the bias current I_b should be increased resulting in a higher current and power consumption. Other options include the use of a class AB OTA [11] or a dynamic/adaptive biasing OTA [12].

Because the cascode transistors M_{3b} and M_{4b} will be rather large, they will add a significant parasitic capacitance to the ouput node that add to the load capacitance C_L. We therefore need to take some margin to account for these additional parasitic capacitances at the output by setting the bias current to $I_b = 250\ nA$ and the inversion coefficient to $IC_1 = 0.1$. The transconductance G_{m1} of M_{1a}-M_{1b} can be calculated from the G_m/I_D function as $G_{m1} = 6.962\ \mu A/V$. This leads to the following gain-bandwidth product $GBW = 1.1\ MHz$, which is slightly higher than the target specification offering some margin. Knowing the drain current I_D and the inversion coefficient IC, we can calculate $I_{spec1} = 2.5\ \mu A$ and $W_1/L_1 = 3.5$. The degree of freedom left (W_1 or L_1) can be determined from the specification on the maximum flicker noise corner frequency

$$f_k = \frac{\rho_n\, G_{m1}}{W_1\, L_1\, \gamma_{n1}} \cdot \frac{1+\eta_{fl}}{1+\eta_{th}}. \tag{3.4}$$

We will assume that $\eta_{th} \ll 1$ and set $\eta_{fl} = 1$. We can then deduce the gate area of M_{1a}-M_{1b} as

$$W_1\, L_1 = \frac{\rho_n\, G_{m1}}{f_k\, \gamma_{n1}} \cdot \frac{1+\eta_{fl}}{1+\eta_{th}}. \tag{3.5}$$

This leads to $W_1\, L_1 = 12.34\ \mu m^2$ and $W_1 = 6.57\ \mu m$ and $L_1 = 1.88\ \mu m$.

We have finalized the sizing of the differential pair M_{1a}-M_{1b}. We can now size the pMOS current mirror M_{2a}-M_{2b}.

3.5 Sizing of M_{2a}-M_{2b}

Because of the transistors stacking, the design of the telescopic OTA becomes tricky at low voltage. The current mirror M_{2a}-M_{2b} should be biased as much in strong inversion as the voltage constraint allows for. We choose to set the quiescent output voltage to $V_{outq} = V_{DD}/2 = 0.9\ V$. The V_{SG2} voltage will set the open-loop quiescent output voltage and is therefore equal to $V_{SG2} = V_{DD} - V_{outq} = 900\ mV$. This corresponds to an inversion coefficient equal to $IC_2 = 40.1$ and a saturation voltage $V_{SDsat2} = 343\ mV$. Having set the inversion coefficient and bias current we can derive $I_{spec2} = 6.24\ nA$ and $W_2/L_2 = 0.036$. Having IC and I_D, we can deduce $G_{m2} = 1.080\ \mu A/V$.

We will now have to make sure that the non-dominant pole f_p at node 2 is sufficiently higher than the gain-bandwidth product GBW to insure the desired phase margin. The non-dominant pole is given by

$$\omega_p = \frac{G_{m2}}{C_2}, \tag{3.6}$$

where C_2 is given by

$$C_2 = 2(C_{GS2} + C_{GB2}) \tag{3.7}$$

Assuming M_{2a}-M_{2b} are biased in saturation, the gate-to-source capacitance C_{GS2} is given by

$$C_{GS2} \cong W_2\, L_2\, C_{ox} \cdot c_{gsi} + C_{GSop} \cdot W_2, \tag{3.8}$$

where C_{GSop} and C_{GSfp} are the gate-to-source overlap and fringing capacitances per unit width for pMOS transistors. c_{gsi} is the intrinsic gate-to-source capacitance normalized to the total gate area $W\,L\,C_{ox}$, which is typically equal to 2/3 in strong inversion and is proportionnal to IC in weak inversion.

The gate-to-bulk capacitance C_{GB2} is given by

$$C_{GB2} \cong\ W_2\, L_2\, C_{ox} \cdot c_{gbi} + C_{GBop} \cdot W_2, \tag{3.9}$$

where C_{GBop} is the gate-to-bulk overlap capacitance per unit width and c_{gbi} is the gate-to-bulk intrinsic capacitance normalized to the total gate area $W\,L\,C_{ox}$ and given by

$$c_{gbi} = \frac{n-1}{n} \cdot c_{gsi}. \tag{3.10}$$

The capacitance at node 2 scales with W_2 and L_2 according to

$$C_2 = C_{WL} \cdot W_2\, L_2 + C_W \cdot W_2, \tag{3.11}$$

with

$$C_{WL} = 2\, C_{ox} \cdot (c_{gsi} + c_{gbi}), \tag{3.12}$$

$$C_W = 2(C_{GSop} + G_{GBop}). \tag{3.13}$$

Since the W/L has already been set by the transconductance and the current, we can derive W_2 and L_2 for achieving a given capacitance C_2 according to

$$W_2 = \frac{-C_W \cdot W_2/L_2 + \sqrt{W_2/L_2} \cdot \sqrt{4\, C_2\, C_{WL} + C_W^2 \cdot W_2/L_2}}{2\, C_{WL}}, \tag{3.14}$$

$$L_2 = \frac{W_2}{W_2/L_2}. \tag{3.15}$$

Setting the non-dominant pole f_p to 10 times the GBW, we get $C_2 = 16$ fF, $L_2 = 6.00\ \mu m$ and $W_2 = 220\ nm$.

We can check the contributions of M_{2a}-M_{2b} to the thermal and flicker noise $\eta_{th} = 0.199$ and $\eta_{fl} = 1.472$. The resulting corner frequency is then given by $f_k = 103.032\ kHz$ which is higher than the specification $f_k = 100\ kHz$ because of the larger $\eta_{fl} =$ compared to the initial value. We can slightly increase the gate area $W_1\,L_1$ of M_{1a}-M_{1b}.

With $W_1\,L_1 = 14.307\ \mu m^2$, the resulting corner frequency is $f_k = 97.555\ kHz$, which is now lower than the specification $f_k = 100\ kHz$.

The new values of W_1 and L_1$ are given by $W_1 = 7.07\ \mu m$ and $L_1 = 2.02\ \mu m$.

3.6 Sizing of M_{3a}-M_{3b} and M_{4a}-M_{4b}

The cascode transistors are sized according to the desired DC gain given by

$$A_{dc} = \frac{G_{m1}}{G_o} \tag{3.16}$$

where G_o is the conductance at the output node given by

$$G_o \cong G_{o1} + G_{o2} \tag{3.17}$$

with

$$G_{o1} = \frac{G_{ds1b} \cdot G_{ds3b}}{G_{ms3b}}, \tag{3.18}$$

$$G_{o2} = \frac{G_{ds2b} \cdot G_{ds4b}}{G_{ms4b}}. \tag{3.19}$$

To have some margin on the DC gain we will design for a minimum DC gain higher than the specification given by $A_{dc} = 100$ dB or $A_{dc} = 1.000\text{e+}05$. We can then deduce the output conductance as $G_o = G_{m1}/A_{dc} = 0.070\ nA/V$. We will split the output conductance G_o equally between the nMOS and pMOS cascodes.

To minimize the saturation voltage and maximize the current efficiency, the cascode transistors M_{3a}-M_{3b} and M_{4a}-M_{4b} are biased in weak inversion. We choose their inversion coefficient as $IC_3 = IC_4 = 0.1$, which gives a saturation voltage $V_{DSsat4} = 105\ mV$. Having set the IC and knowing the bias current, we can deduce $I_{spec3} = 2.5\ \mu A$ and $W_3/L_3 = 3.496$ for M_{3a}-M_{3b} and $I_{spec4} = 2.5\ \mu A$ and $W_4/L_4 = 14.440$ for M_{4a}-M_{4b}. We can now calculate the G_{ms} that is needed for the calculation of the output conductances $G_{ms3} = 8.851\ \mu A/V$ and $G_{ms4} = 8.851\ \mu A/V$. Having already the length of M_{2a}-M_{2b}, we can estimate its output conductance G_{ds2} as $G_{ds2} = 2.083\ nA/V$. We can then deduce the output conductance G_{ds4} of M_{4a}-M_{4b} as $G_{ds4} = 147.9\ nA/V$, which corresponds to a cascode gain $G_{ms4}/G_{ds4} = 59.9$. We can deduce the length of M_{4a}-M_{4b} from G_{ds4} as $L_4 = 80\ nm$, which is smaller than L_{min}.

In order not to degrade the output conductance, we choose L_4 to be 3 times L_{min} resulting in $L_4 = 540\ nm$, which gives a width equal to $W_4 = 7.80\ \mu m$. We can re-estimate the output conductances $G_{o2} = 0.005\ nA/V$ giving $G_{o1} = 0.064\ nA/V$.

Since we already know the length $L_1 = 2.02\ \mu m$ and the current $I_b = 250\ nA$ for M_{1a}-M_{1b}, we can estimate its output conductance $G_{ds1} = 6.188\ nA/V$. The output conductance of M_{3a}-M_{3b} is then given by $G_{ds3} = 91.784\ nA/V$ from which we can deduce its length $L_3 = 136\ nm$ and its width $W_3 = 0.48\ \mu m$.

In order to maximize the DC gain we will choose $L_3 = 540\ nm$. Keeping the same W/L results in $W_3 = 1.89\ \mu m$. The DC gain is now $A_{dc} = 110.152$ dB.

3.7 Sizing M_{5a}-M_{5b}

The sizing of M_{5a}-M_{5b} is conditioned by the minimum input common-mode voltage keeping M_{5a}-M_{5b} in saturation

$$V_{ic,min} = V_{GS1} + V_{DSsat5} \tag{3.20}$$

The gate-to-source voltage V_{GS1} is given by

$$V_{GS1} = V_{T0n} + (n_{0n} - 1)\, V_{S1} + n_{0n}\, U_T\, (v_p - v_s) \tag{3.21}$$

Since M_{1a}-M_{1b} are in a separate well $V_{SB1} = 0$. Additionally in weak inversion we can consider $v_p - v_s \cong 0$. V_{GS1} can therefore be approximated by $V_{GS1} \cong V_{T0n}$. This gives $V_{GS1} = 455\ mV$, which for $V_{ic} = V_{DD}/2 = 900\ mV$ leaves $V_{DS3} = 445\ mV$. If we set the saturation voltage of M_{5a}-M_{5b} to $V_{DSsat5} = 300\ mV$, this corresponds to an inversion coefficient $IC_5 = 29.6$. Having the IC and the current we can derive $I_{spec5} = 17\ nA$ and $W_5/L_5 = 0.024$. Since W_5/L_5 is small, we need to set W_5 to $W_5 = W_{min} = 200\ nm$ resulting in $L_5 = 8.47\ \mu m$. Note that the minimum input common-mode voltage is then given by $V_{ic,min} = 755\ mV$.

We still need to calculate the required bias voltages V_{b1} for M_{3a}-M_{3b} and V_{b2} for M_{4a}-M_{4b} which is done in the next section.

3.8 Bias voltages V_{b1} and V_{b2}

We start calculating the maximum bias voltage $V_{b2,max}$ still keeping M_{2a}-M_{2b} in saturation

$$V_{b2,max} = V_{DD} - V_{SG4} - V_{SDsat2} \tag{3.22}$$

with $V_{SG4} = 445\ mV$ and $V_{SDsat2} = 343\ mV$, we get $V_{b2,max} = 1.012\ V$.

We also want to make sure that the V_{SD} voltage across M_{4a}-M_{4b} is large enough not to degrade its output conductance

$$V_{b2,min} = V_{SD4} - V_{SG4} + V_{DD} - V_{SG2}. \tag{3.23}$$

Setting the source-to-drain voltage of M_{4a}-M_{4b} to $V_{SD4} = 200\ mV$, with $V_{SG4} = 445\ mV$ and $V_{SG2} = 900\ mV$, we get $V_{b2,min} = 0.655\ V$.

Similarly, we can calculate the maximum bias voltage $V_{b1,max}$ allocating enough V_{DS} voltage for M_{3a}-M_{3b} not to degrade its output conductance. This leads to

$$V_{b1,max} = V_{GS3} - V_{DS3} - V_{SG2} + V_{DD}. \tag{3.24}$$

Allocating $V_{DS3} = 200\ mV$, with $V_{GS3} = 455\ mV$ and $V_{SG2} = 900\ mV$, we get $V_{b1,max} = 1.155\ V$.

We also want to make sure that the V_{DS} voltage of M_{1a}-M_{1b} is large enough not to degrade its output conductance. This sets a minimum value for V_{b1} given by

$$V_{b1,min} = V_{GS3} + V_{DS1} - V_{GS1} + V_{ic}. \tag{3.25}$$

For $V_{ic} = 0.9\ V$ and $V_{DS1} = 200\ mV$, with $V_{GS1} = 455\ mV$, we get $V_{b1,min} = 1.100\ V$

> **Note**
>
> Setting V_{b1} and V_{b2} is tricky and requires a bit of fine tuning. After checking by simulation, we finally choose $V_{b1} = 1.200\ V$ and $V_{b2} = 0.700\ V$.

The design is now finalized. The transistor sizes and bias are summarized below.

3.9 Summary

3.9.1 Specifications

The specifications are recalled in Table 3.5.

Table 3.5: OTA specifications.

Specification	Symbol	Value	Unit
Minimum DC gain	A_{dc}	100	dB
Minimum gain-bandwidth product	GBW	1	MHz
Load capacitance	C_L	1	pF
Maximum input-referred random offset voltage	V_{os}	10	mV
Phase margin	PM	60	$^\circ$
Corner frequency	f_k	100	kHz

3.9.2 Bias

The bias information are summarized in Table 3.6.

Table 3.6: OTA bias.

Bias voltage or current	Symbol	Value	Unit
Supply voltage	V_{DD}	1.8	V
Bias current	I_b	250.0	nA
Cascode bias voltage	V_{b1}	1.2	V
Cascode bias voltage	V_{b2}	0.7	V

3.9.3 Transistor information

The transistor sizes and large-signal variables are summarized in Table 3.7, whereas Table 3.8 gives the small-signal and thermal noise parameters. An Excel table is generated with more information (e.g. all the parasitic capacitances).

Table 3.7: Transistor size and bias information.

Transistor	W $[\mu m]$	L $[\mu m]$	I_D $[nA]$	I_{spec} $[nA]$	IC	$V_G - V_{T0}$ $[mV]$	V_{DSsat} $[mV]$
M1a	7.07	2.02	250	2503	0.1	-45	105
M1b	7.07	2.02	250	2503	0.1	-45	105
M2a	0.22	6.00	250	6	39.4	264	341
M2b	0.22	6.00	250	6	39.4	264	341
M3a	1.89	0.54	250	2503	0.1	-45	105
M3b	1.89	0.54	250	2503	0.1	-45	105
M4a	7.80	0.54	250	2501	0.1	-44	105
M4b	7.80	0.54	250	2501	0.1	-44	105
M5a	0.20	8.47	500	17	29.6	235	300
M5b	0.20	8.47	500	17	29.6	235	300

Table 3.8: Transistor small-signal and thermal noise parameters.

Transistor	G_{spec} $[\mu A/V]$	G_{ms} $[\mu A/V]$	G_m $[\mu A/V]$	G_{ds} $[nA/V]$	γ_n
M1a	96.716	8.852	6.962	6.188	0.653
M1b	96.716	8.852	6.962	6.188	0.653
M2a	0.245	1.422	1.089	2.083	0.839
M2b	0.245	1.422	1.089	2.083	0.839
M3a	96.716	8.852	6.962	23.148	0.653
M3b	96.716	8.852	6.962	23.148	0.653
M4a	96.650	8.851	6.777	23.148	0.671
M4b	96.650	8.851	6.777	23.148	0.671
M5a	0.652	3.240	2.548	2.952	0.812
M5b	0.652	3.240	2.548	2.952	0.812

4 OTA Characteristics

In this section, we check whether the specs are achieved.

4.1 Open-loop gain

We can calculate the various OTA features related to the open-loop transfer function, which are given in Table 4.1.

Table 4.1: OTA gain variables.

Symbol	Theoretical Value	Unit
A_{dc}	110.154	dB
G_{m1}	6.962	$\mu A/V$
G_{ds1}	6.188	nA/V
G_{m2}	1.089	$\mu A/V$
G_{ds2}	2.083	nA/V
G_{ms3}	8.852	$\mu A/V$
G_{ds3}	23.148	nA/V
G_{ms4}	8.851	$\mu A/V$
G_{ds4}	23.148	nA/V
C_2	15.784	fF
f_0	3.424	Hz
GBW	1.102	MHz
f_p	10.977	MHz
f_z	21.954	MHz

The gain-bandwidth product from the specifications is repeated here

$GBW = 1.000$ MHz (from spec).

The estimate value assuming that all the non-dominant poles are much higher than the GBW is given by

$GBW_{est} = 1.102$ MHz (estimation).

The GBW accounting for the effect of the additional non-dominant poles is given by

$GBW_{the} = 1.098$ MHz (theory).

We see that there is only a small difference between GBW_{est} and GBW_{the}, which confirms that the non-dominant poles are sufficiently far from GBW as stated in Table 4.1.

We can now plot the gain response Using the variables given in Table 4.1. It is shown in Figure 4.1.

From Figure 4.1, we see that the GBW is right on target and the DC gain is much larger than the specification.

We can now have a look at the input-referred noise PSD.

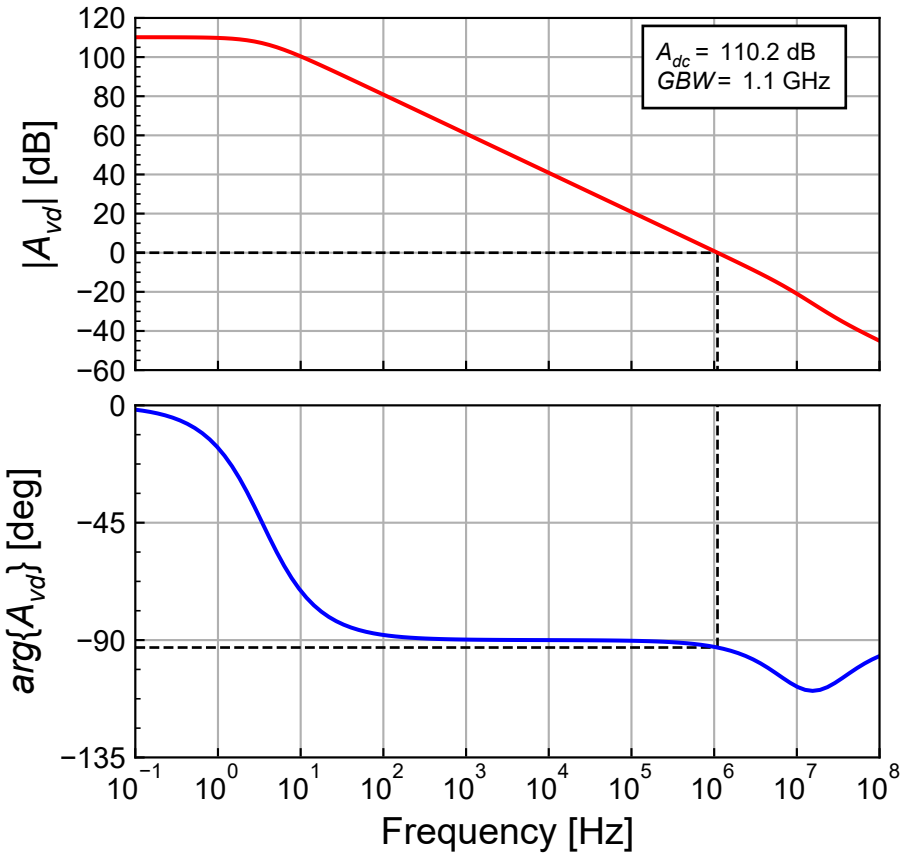

Figure 4.1: OTA theoretical transfer function.

4.2 Input-referred noise

We can compute all the parameters needed for the calculation of the OTA thermal noise excess factor and its input-referred thermal noise PSD and resistance. They are given in Table 4.2.

Table 4.2: OTA thermal noise parameters.

Symbol	Theoretical Value	Unit
G_{m1}	6.962	$\mu A/V$
G_{m2}	1.089	$\mu A/V$
G_{m1}/G_{m2}	6.395	-
γ_{n1}	0.653	-
γ_{n2}	0.839	-
η_{th}	0.201	-
γ_{ota}	1.569	-
R_{nt}	225.378	$k\Omega$
$\sqrt{S_{ninth}}$	61.092	$nV/\sqrt{Hz}$
$10 \cdot \log(S_{ninth})$	-144.280	$dBv/\sqrt{Hz}$

From Table 4.2, we see that the OTA thermal noise excess factor $\gamma_{ota} = 1.569$ is only slightly larger than that of the differential pair $2\,\gamma_{n1} = 1.307$. This is due to the low value of $\eta_{th} = 0.201$ indicating that the current mirror M_{2a}-M_{2b} is contributing about half the contribution of the differential pair M_{1a}-M_{1b}.

We can now compute all the parameters needed for the calculation of the input-referred flicker noise and the corner frequency. They are given in Table 4.3.

Table 4.3: OTA flicker noise parameters.

Symbol	Theoretical Value	Unit	Comment
$(G_{m1}/G_{m2})^2$	40.900	-	
ρ_p/ρ_n	8.333	-	
$\frac{W_1 \cdot L_1}{W_2 \cdot L_2}$	8.508	-	
η_{fl}	1.734	-	
$\sqrt{S_{ninfl}(1\,Hz)}$	19.482	$\mu V/\sqrt{Hz}$	
$10 \cdot \log(S_{ninfl}(1\,Hz))$	-94.207	$dBv/\sqrt{Hz}$	
$(1+\eta_{fl})/(1+\eta_{th})$	2.277	-	
f_k	43.224	kHz	Differential pair only
f_k	98.406	kHz	

From Table 4.3, we see that $\eta_{fl} = 1.734$, which means that the contribution of the current mirror M_{2a}-M_{2b} to the input-referred flicker noise is about the same as the differential pair M_{1a}-M_{1b} despite the flicker of pMOS transistor is higher by a factor $\rho_p/\rho_n = 8.333$ for the same gate area. We also see that the corner frequency is lower than the specification due to the fact that we have increased the length of M_{1a}-M_{1b} for achieving the DC gain.

We can plot the input-referred noise which is shown in Figure 4.2.

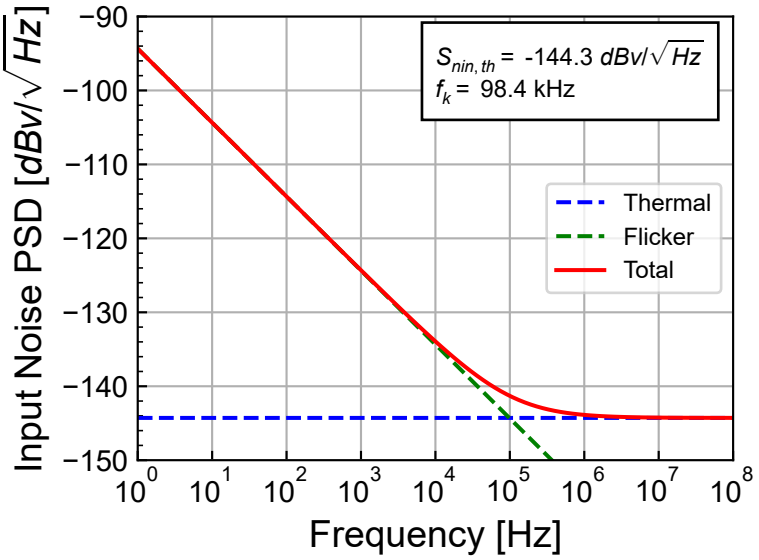

Figure 4.2: OTA theoretical input-referred noise PSD.

4.3 Input-referred offset

The variance of the input-referred offset voltage is given by (2.33), which is repeated below

$$\sigma^2_{V_{os}} = \sigma^2_{V_T} + \sigma^2_{\beta}, \tag{4.1}$$

where

$$\sigma^2_{V_T} = \sigma^2_{V_{T1}} \cdot (1 + \xi_{V_T}) \tag{4.2}$$

is the V_T-mismatch and

$$\sigma_\beta^2 = \left(\frac{I_b}{G_{m1}}\right)^2 \cdot \sigma_{\beta_1}^2 \cdot (1 + \xi_\beta) \tag{4.3}$$

is the β-mismatch with

$$\sigma_{V_{T1}} = \frac{A_{V_{Tn}}^2}{W_1\, L_1} \tag{4.4}$$

and

$$\sigma_{\beta_1}^2 = \frac{A_{\beta_n}^2}{W_1\, L_1}. \tag{4.5}$$

ξ_{V_T} represents the V_T-mismatch contribution to the input-referred offset of the current mirror relative to that of the differential pair. It is given by (2.40) which is repeated below

$$\xi_{V_T} = \left(\frac{G_{m2}}{G_{m1}}\right)^2 \cdot \left(\frac{A_{V_{Tp}}}{A_{V_{Tp}}}\right)^2 \cdot \frac{W_1\, L_1}{W_2\, L_2}. \tag{4.6}$$

ξ_β represents the β-mismatch contributions to the input-referred offset of the current mirror relative to that of the differential pair. It is given by (2.41) which is repeated below

$$\xi_\beta = \left(\frac{A_{\beta_p}}{A_{\beta_n}}\right)^2 \cdot \frac{W_1\, L_1}{W_2\, L_2}. \tag{4.7}$$

The parameter for calculating the standard deviation of the input-referred offset voltage are given in Table 4.4.

Table 4.4: OTA input-referred offset parameters.

Symbol	Theoretical Value	Unit
σ_{VT1}	1.323	mV
σ_{VT2}	4.352	mV
$\sigma_{\beta 1}$	0.265	%
$\sigma_{\beta 2}$	0.870	%
ξ_{VT}	0.265	-
ξ_β	10.819	-
$\sigma_{V_T}^2$	2.214	mV^2
σ_{V_T}	1.488	mV
σ_β^2	0.107	mV^2
σ_β	0.327	mV
σ_{Vos}	1.523	mV

From Table 4.4, we see that the β-mismatch is negligible and that the input-referred offset voltage is dominated by the contribution of the V_T-mismatch from the differential pair.

4.4 Current and power consumption

The total current consumption, ignoring the current drawn by M_{5a}, is $I_{tot} = 2I_b = 0.5\ \mu A$. Assuming the input differential pair M_{1a}-M_{1b} is biased in deep weak inversion, the minimum bias current is directly related to the gain-bandwidth product GBW according to

$I_{b,min} \cong nU_T \cdot C_L \cdot \omega_u = nU_T \cdot C_L \cdot 2\pi\, GBW = 207\ nA.$

The minimum total current consumption can then be estimated as $I_{tot,min} \cong 2I_{b,min} = 413\ nA$. The actual current consumption accounting for some margin taken on the GBW is therefore 21% higher than the minimum.

> **Note**
>
> Note that the telescopic OTA is the differential OTA that has the minimum power consumption for similar gain-bandwidth product, DC gain and phase margin specifications. Of course it has the smallest input and output voltage swings.

The above design will now be checked against simulations.

5 Simulation results from ngspice

The theoretical results can be validated with the results obtained from simulations performed with ngspice. In order to run the simulations you need to have ngspice correctly installed. Please refer to the installation instructions.

> **Note**
>
> The simulations are performed with ngspice [5] using the EKV 2.6 compact model [6] [13] [2]. For ngspice, we use the original Verilog-A implementation of EKV 2.6 [8] modified by C. Enz to get the operating point informations and available on the Gitub va-models site provided by D. Warning at [7] [14]. The Verilog-A code was then compiled with OpenVAF [15] to generate the OSDI for running it with ngspice. The parameters correspond to a generic 180 nm bulk CMOS process [9].

5.1 Operating point

We first write the parameter file for this specific design for running the ngspice simulations. Before running the AC and NOISE simulations, we first need to check the quiescent voltages and currents and the operating points of all transistors by running a .OP simulation.

Table 5.1: OTA node voltages with the OTA in open-loop without offset correction.

Node	Voltage
vdd	1.800
vb1	1.200
vb2	0.700
inp	0.900
inn	0.900
out	0.905
ic	0.900
id	0.000
1	0.402
2	0.905
3	0.628
4	0.628
5	1.264
6	1.264
7	0.821
8	0.399

We can extract the OTA quiescent node voltages from the ngspice .ic file. They are presented in Table 5.1. We see that the simulated quiescent output voltage $V_{outq} = 905\ mV$ is close to the desired value set at $V_{outq} = 900\ mV$. This means that the OTA is biased in the high gain region and we

actually don't need to extract any offset voltage at this point and can proceed with the simulation of the large-signal characteristic.

The operating point information for all transistors are extracted from the ngspice .op file. The data is split into the large-signal operating informations in Table 5.2, the small-signal operating point informations in Table 5.3 and the noise operating point informations in Table 5.4.

Table 5.2: Operating point information extracted from ngspice .op file for each transistor.

Transistor	I_D $[nA]$	I_{spec} $[nA]$	IC	n	V_{Dsat} $[mV]$
M1a	250	2355	0.106	1.27	120
M1b	250	2355	0.106	1.27	120
M2a	250	7	38.417	1.31	424
M2b	250	7	38.417	1.31	424
M3a	250	2584	0.097	1.27	120
M3b	250	2584	0.097	1.27	120
M4a	250	2367	0.106	1.31	120
M4b	250	2367	0.106	1.31	120
M5a	500	18	28.507	1.27	380
M5b	500	18	28.507	1.27	380

Table 5.3: Small-signal operating point information extracted from ngspice .op file for each transistor.

Transistor	n	G_{ms} $[\mu A/V]$	G_m $[\mu A/V]$	G_{mb} $[\mu A/V]$	G_{ds} $[nA/V]$
M1a	1.27	8.801	7.081	1.709	11.230
M1b	1.27	8.801	7.081	1.709	11.230
M2a	1.31	1.414	1.039	0.374	1.144
M2b	1.31	1.414	1.039	0.374	1.144
M3a	1.27	8.838	7.252	1.548	38.346
M3b	1.27	8.838	7.252	1.548	38.346
M4a	1.31	8.812	6.979	1.813	19.518
M4b	1.31	8.812	6.979	1.813	19.518
M5a	1.27	3.209	2.477	0.717	15.162
M5b	1.27	3.209	2.478	0.717	13.987

Table 5.4: Noise operating point information extracted from ngspice .op file for each transistor.

Transistor	γ_n	$R_{n,th}$ $[k\Omega]$	$V_{n,th}$ $[nV/\sqrt{Hz}]$	$V_{n,fl}$ at 1Hz $[\mu V/\sqrt{Hz}]$
M1a	0.65	91.2	38.9	8.3
M1b	0.65	91.2	38.9	8.3
M2a	0.90	865.2	119.8	70.1
M2b	0.90	865.2	119.8	70.1
M3a	0.63	87.2	38.0	32.7
M3b	0.63	87.2	38.0	32.7
M4a	0.65	93.8	39.4	46.6
M4b	0.65	93.8	39.4	46.6
M5a	0.86	346.5	75.8	21.8
M5b	0.86	346.2	75.8	21.8

We can also check the bias voltages and operating region of each transistor which are given in Table 5.5.

Table 5.5: Bias voltages and operating regions extracted from ngspice for each transistor.

Trans.	Type	Funct.	V_G [V]	V_S [V]	V_D [V]	V_{DS} [mV]	V_{Dsat} [mV]	Reg.	Sat.
M1a	n	DP	0.900	0.402	0.628	227	120	MI	sat
M1b	n	DP	0.900	0.402	0.628	227	120	MI	sat
M2a	p	CM	0.895	0.000	0.536	536	424	SI	sat
M2b	p	CM	0.895	0.000	0.536	536	424	SI	sat
M3a	n	CA	1.200	0.628	0.905	276	120	WI	sat
M3b	n	CA	1.200	0.628	0.905	276	120	WI	sat
M4a	p	CA	1.100	0.536	0.895	360	120	MI	sat
M4b	p	CA	1.100	0.536	0.895	360	120	MI	sat
M5a	n	CM	0.821	0.000	0.399	399	380	SI	sat
M5b	n	CM	0.821	0.000	0.402	402	380	SI	sat

From Table 5.2, we see that all transistors have a sufficiently large V_{DS} voltage and are therefore biased in saturation. Additionnally we see that all the saturation voltages in the output current branch M_{2d}, M_4, M_7 and M_{3b} are summing up to 1164 mV leaving an output voltage swing about equal to $V_{out,swing} \cong 636\ mV$. This output voltage swing could be increased by about 250 mV by biasing M_{2d} and M_{3b} in weak inversion. This would be at the cost of larger transistors and a less current matching in the current mirrors.

From Table 5.5, we see that all transistors are biased in saturation. The operating points look fine. We can now proceed with the simulation of the open-loop large-signal transfer characteristic.

5.2 Large-signal differential transfer characteristic

We now simulate the DC differential transfer characteristic. The simulation of the large-signal input-output characteristic is presented in Figure 5.1.

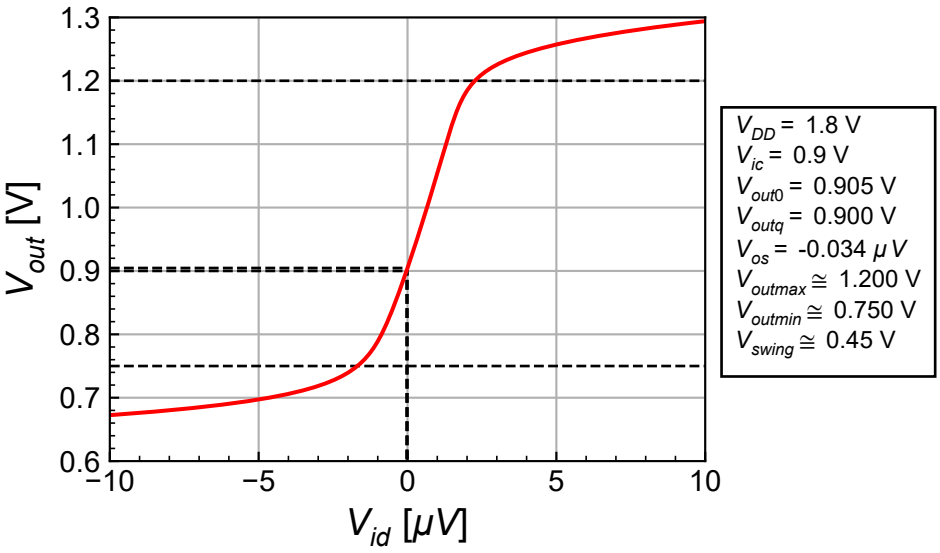

Figure 5.1: Simulated large-signal input-output characteristic.

From Figure 5.1, we see that the output swing is about $V_{out,swing} \cong 450\ mV$, which is even less than the above estimation. We can now zoom into the high gain region in order to extract the offset voltage that is needed to bring the output voltage back to $V_{outq} = 0.900\ V$. The simulation results are presented in Figure 5.2.

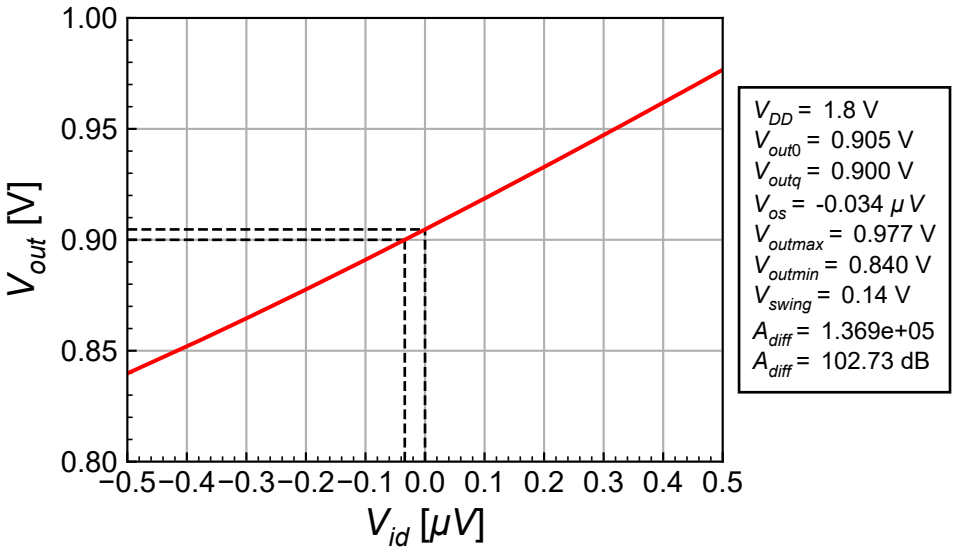

Figure 5.2: Zoom of the simulated large-signal input-output characteristic in the gain region.

We can now save the extracted offset voltage V_{os} = -0.034 μV that is required to bring the output voltage to $V_{outq} = 0.900\ V$ and that will be used for the following .AC and .NOISE simulations.

5.3 Open-loop gain

After having checked the operating point information and making sure that the OTA output is not saturated by extracting the required offset voltage for bringing the output operating point to the desired value $V_{outq} = 0.900\ V$, we can now perform the AC simulation. The open-loop transfer function is shown in Figure 5.3.

From Figure 5.3, we see that the simulated differential gain magnitude is very close to the theoretical estimation. The simulated GBW is euqual to the predicted GBW and above specification. The simulated DC gain is sligtly lower than the theoretical estimation. This difference is obviously due to the poor output conductance model we have used for the design.

5.4 Input-referred noise

The simulated input-referred noise PSD is presented in Figure 5.4 and compared to the theoretical estimation.

From Figure 5.4, we see that there is a perfect match between the simulated and estimated input-referred noise PSD for both the white and flicker noise PSD. We also observe that the specification of the corner frequency is met. The discrepancy appearing at high frequency is simply due to the fact that the theoretical input-referred noise was obtained by dividing the output noise current PSD by the square of the equivalent transconductance without accounting for its frequency dependence. We can have a closer look at the contributions of the various transistors to the input-referred noise PSD.

Figure 5.5 shows that the simulated total input-referred white noise PSD perfectly matches the theoretical prediction. Figure 5.5 also shows the contributions of M_{1a}-M_{1b}, M_{2a}-M_{2b}, M_{3a}-M_{3b}, M_{4a}-M_{4b} and M_{5a}-M_{5b} to the input-referred white noise PSD. We can oberve that the white noise is dominated by the contribution of M_{1a}-M_{1b}. This is confirmed by the value of the simulated η_{th} = 0.205 which is very close to the theoretical value $\eta_{th} = 0.201$. The contribution of M_{2a}-M_{2b} is 6.9 dB lower than the contribution of M_{1a}-M_{1b}. We also see that the contributions of the cascode transistors

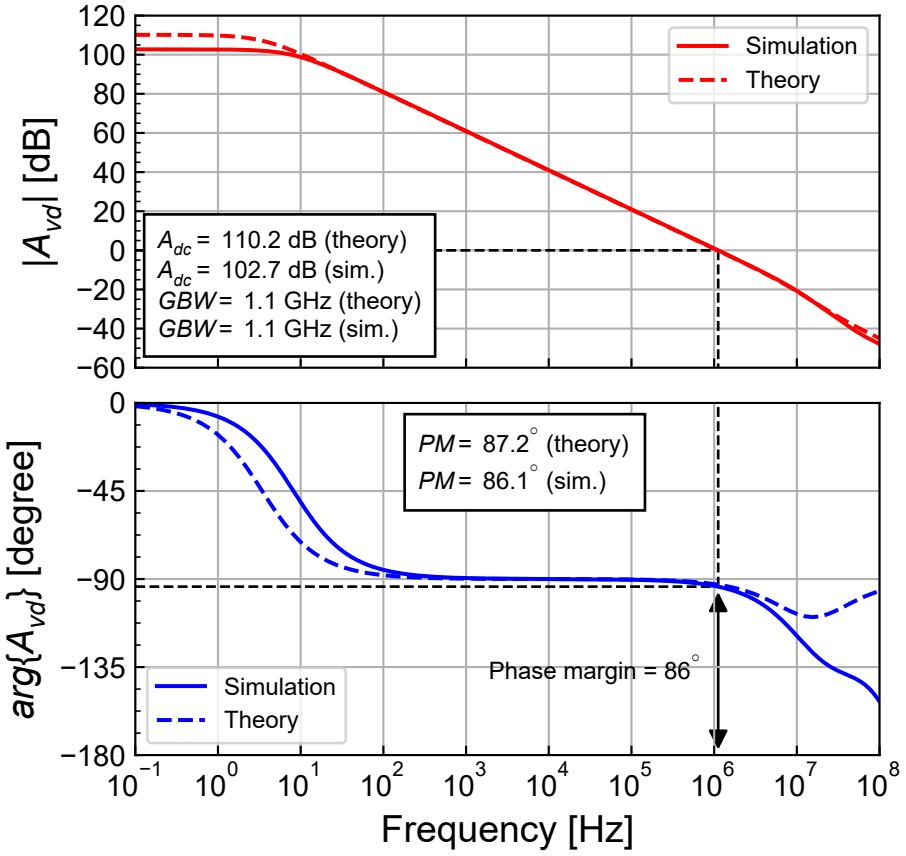

Figure 5.3: Simulated gain response compared to theoretical estimation.

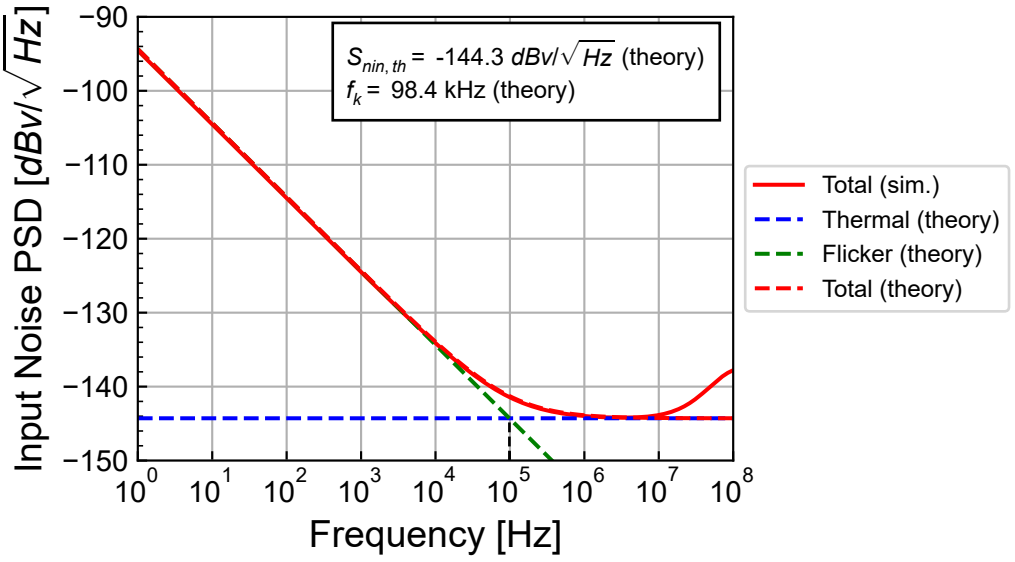

Figure 5.4: Simulated input-referred noise PSD compared to theoretical estimation.

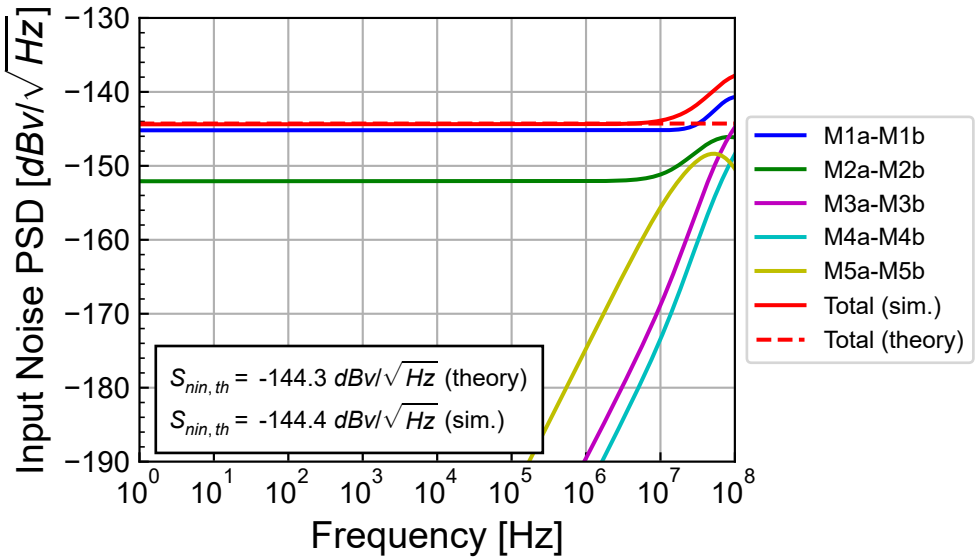

Figure 5.5: Breakdown of the contributions to the simulated input-referred white noise PSD.

M_{3a}-M_{3b} and M_{4a}-M_{4b} are negligible. The contribution of M_{5a}-M_{5b} is also negligible since it is a common mode contribution which is cancelled at the output. Finally, the simulated OTA thermal noise excess factor $\gamma_{n,ota} = 1.558$ is slightly smaller than the predicted value $\gamma_{n,ota} = 1.569$.

Figure 5.6 presents the breakdown of the contributions of the various transistors to the input-referred flicker noise.

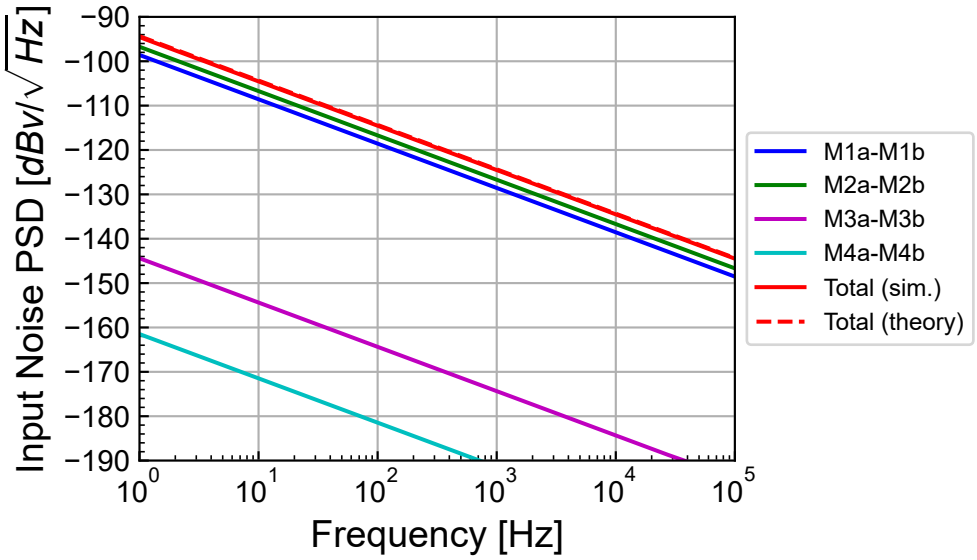

Figure 5.6: Breakdown of the contributions to the simulated input-referred flicker noise PSD.

Similarly to the white noise, Figure 5.6 shows that the total simulated input-referred flicker noise PSD perfectly matches the theoretical prediction. We can observe that the input-referred flicker noise is dominated by the contribution of M_{2a}-M_{2b} which is 1.845 dB higher than the contribution of M_{1a}-M_{1b}. This consistent with the value of $\eta_{fl} = 1.529$ (1.845 in dB) which is close to the theoretical value $\eta_{fl} = 1.734$. We see that M_{2a}-M_{2b} contribute about the same than M_{1a}-M_{1b} and that the contributions of the cascode transistors M_{3a}-M_{3b} and M_{4a}-M_{4b} are negligible. The contributions of the cascode transistors is negligible. Note that the contribution of M_{5a}-M_{5b} is not shown because it is completely negligible.

The contributions of the various transistors to the total input-referred noise PSd is shown in Figure 5.7.

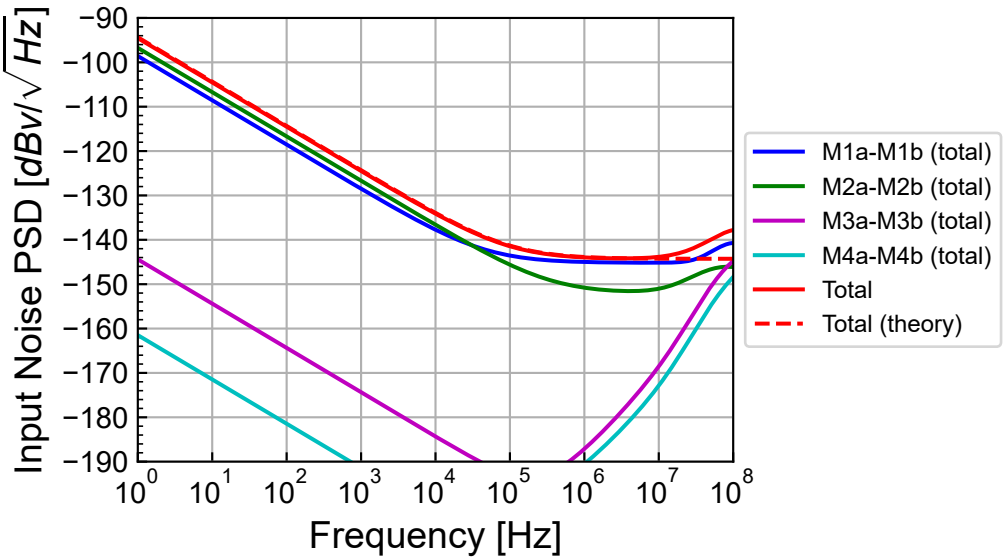

Figure 5.7: Breakdown of the contributions to the simulated input-referred noise PSD.

5.5 Input common-mode voltage range

We can check the input common-mode voltage range by connecting the OTA as a voltage follower and sweeping the positive input.

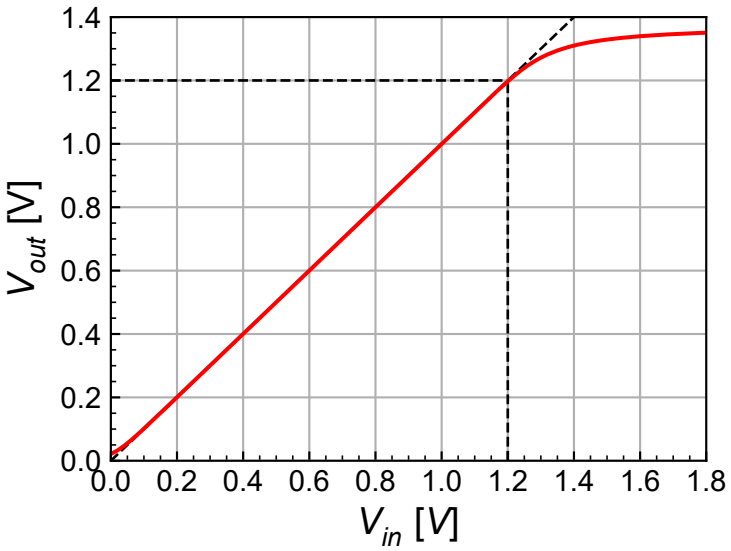

Figure 5.8: Simulated input common-mode voltage range.

As shown in Figure 5.8, the output follows the input voltage up to 1.2 V. So the input common-mode voltage range is about 1.2 V.

5.6 Step-response

In this section we will check the step response of the OTA operating as a voltage follower as shown in Figure 5.9 with its output connected to the negative input and with the same load capacitance $C_L = 1$ pF.

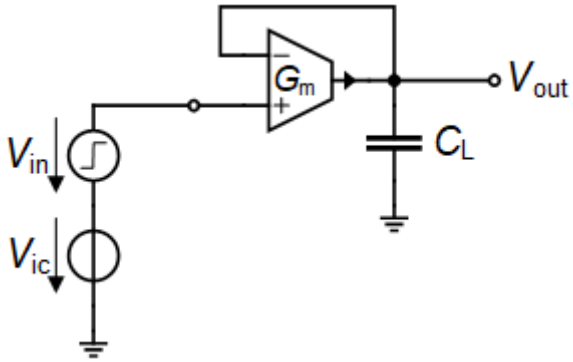

Figure 5.9: Schematic of the OTA connected as a voltage follower.

5.6.1 Small-step

According to the input common-mode voltage range established above, we will set the input common-mode voltage to $V_{ic} = 0.900\ V$ to make sure that the OTA is in the high gain region. We start by imposing a small step $\Delta V_{in} = 10\ mV$ on top of a common mode voltage $V_{ic} = 0.900\ V$. The simulation results are shown in Figure 5.10 where $\Delta V_{in}(t) \triangleq V_{in+}(t) - V_{ic}$ and $\Delta V_{out}(t) \triangleq V_{out}(t) - V_{outq}$ with $V_{outq} \cong V_{ic}$ is the quiescent output voltage. ΔV_{in} and ΔV_{out} are compared to the response of a single pole circuit having a cut-off frequency equal to the GBW. From Figure 5.10, we see that the simulation result is very close to the first-order response.

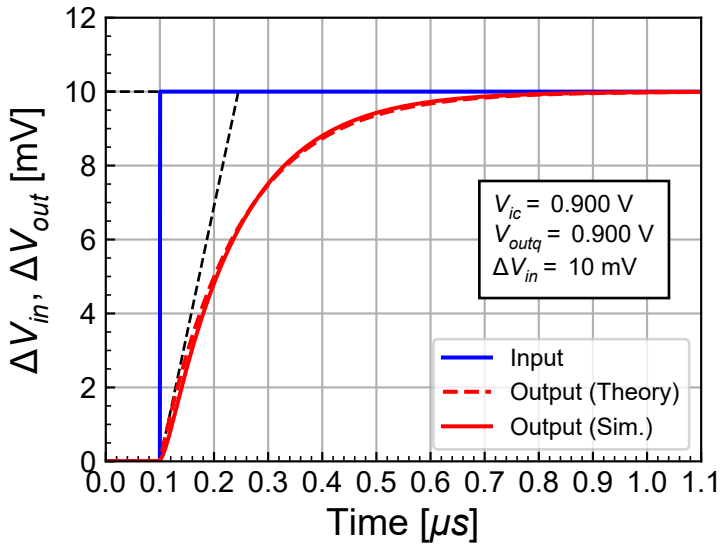

Figure 5.10: Step response of the OTA connected as a voltage follower for a small input step.

5.6.2 Large step

Since we now impose a larger step $\Delta V_{in} = 300\ mV$, we need to lower the input common-mode voltage to $V_{ic} = 800\ mV$, to make sure that after the step the OTA remains in the high gain region and correctly settles to the right voltage. The simulation results are shown in Figure 5.11 where $\Delta V_{in}(t) \triangleq V_{in+}(t) - V_{ic}$ and $\Delta V_{out}(t) \triangleq V_{out}(t) - V_{outq}$ with $V_{outq} \cong V_{ic}$ is the quiescent output voltage. ΔV_{in} and ΔV_{out} are compared to the response of a single pole circuit having a cut-off frequency equal to the GBW. We now observe the effect of slew-rate which increases the settling time.

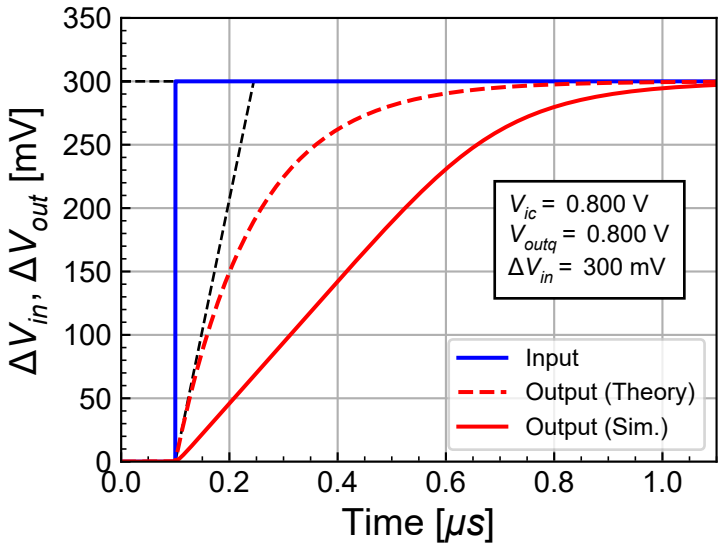

Figure 5.11: Step response of the OTA connected as a voltage follower for a large input step highlighting the slew-rate effect.

5.7 Power consumption

The total current consumption, ignoring the current drawn by M_{5a}, is $I_{tot} = 2I_b = 0.5\ \mu A$ and the total power consumption is then $P = 0.9\ \mu W$. Assuming the input differential pair M_{1a}-M_{1b} is biased in deep weak inversion, the minimum bias current is directly related to the gain-bandwidth product GBW according to

$$I_{b,min} \cong nU_T \cdot C_L \cdot \omega_u = nU_T \cdot C_L \cdot 2\pi\, GBW = 207\ nA.$$

The minimum total current consumption can then be estimated as $I_{tot,min} \cong 2I_{b,min} = 413\ nA$. The actual current consumption accounting for some margin taken on the GBW is therefore 21% higher than the absolute minimum. Note that this increased current consumption is necessary to fight against the paraistic capciatnces at the OTA output.

> **Note**
>
> Note that the telescopic OTA is the differential OTA that has the minimum power consumption for similar gain-bandwidth product, DC gain and phase margin specifications. Of course it has the smallest input and output voltage swings and the DC gain equivalent to the two-stage OTA is hard to achieve at low-voltage.

6 Conclusion

This notebook presented the analysis, design and verification of the telescopic OTA [1] designed for a generic 180nm bulk CMOS process. The detailed analysis provided all the equations that were then used in the design phase to reach the target specifications. The design was then performed using the inversion coefficient approach with the sEKV transistor model [2] [3] [4]. The theoretical performance resulting from the design were then evaluated.

The design was then verified by simulation using ngspice [5] with the EKV 2.6 compact model [6] and the parameters of a generic 180 nm bulk CMOS process. After carefully checking the operating point, the large-signal transfer characteristic was simulated. The small-signal open-loop transfer function was then simulated making sure the OTA was biased in the high gain region. The simulated transfer function was very close to the theoretical prediction except for the DC gain which is slightly smaller but still in spec. The simulations have also shown that the gain-bandwidth product GBW and the DC gain specifications are both achieved.

The input-referred noise was then simulated. The total simulated input-referred noise PSD perfectly matches the theoretical estimation for both the white noise and the flicker noise. The simulations have also shown that the specification on the corener frequency was met. The contributions of the various transistors to the input-referred white noise were then extracted from the noise simulation and compared to the theoretical estimation. It was shown that the total white noise is very close to the theoretical estimation. The simulation of the input-referred flicker noise have shown that it is dominated by the current mirror M_{2a}-M_{2b}. Finally, the simulations have confirmed that the noise contributions of the cascode transistors are completely negligible.

The input common-mode voltage range was then simulated with the OTA connected as a voltage follower. The input voltage is limited to 1.2 V.

Finally, the small-signal step response was simulated and succesfully compared to the response of a single-pole system. The step-response with a large input step highlighted the effect of slew-rate.

The telescopic OTA is the most power efficient differential OTA among those we have studied. This efficiency comes at the cost of a reduced input and output voltage swing and lower DC gain at lower supply voltage.

References

[1] B. Razavi, *Design of Analog CMOS Integrated Circuits*, 2nd ed. Mc-Graw-Hill, 2017.

[2] C. C. Enz and E. A. Vittoz, *Charge-Based MOS Transistor Modeling - The EKV Model for Low-Power and RF IC Design*, 1st ed. John Wiley, 2006.

[3] C. Enz, F. Chicco, and A. Pezzotta, "Nanoscale MOSFET Modeling: Part 1: The Simplified EKV Model for the Design of Low-Power Analog Circuits," *IEEE Solid-State Circuits Magazine*, vol. 9, no. 3, pp. 26–35, 2017.

[4] C. Enz, F. Chicco, and A. Pezzotta, "Nanoscale MOSFET Modeling: Part 2: Using the Inversion Coefficient as the Primary Design Parameter," *IEEE Solid-State Circuits Magazine*, vol. 9, no. 4, pp. 73–81, 2017.

[5] Holger Vogt, Giles Atkinson, Paolo Nenzi, "Ngspice User's Manual Version 43." https://ngspice.sourceforge.io/docs/ngspice-43-manual.pdf, 2024.

[6] M. Bucher, C. Lallement, C. Enz, F. Théodoloz, and F. Krummenacher, "The EPFL-EKV MOSFET Model Equations for Simulation." https://github.com/chrisenz/EKV/blob/main/EKV2.6/docs/ekv_v26_rev2.pdf, 1998.

[7] M. Bucher, C. Lallement, C. Enz, F. Théodoloz, and F. Krummenacher, "EKV 2.6 Verilog-A Code." https://github.com/chrisenz/EKV/tree/main/EKV2.6/va/code, 2024.

[8] W. Grabinski *et al.*, "FOSS EKV2.6 verilog-a compact MOSFET model," in *European solid-state device research conference (ESSDERC)*, 2019, pp. 190–193. doi: 10.1109/ESSDERC.2019.8901822.

[9] W. Grabinski *et al.*, "FOSS EKV 2.6 parameter extractor," in *2015 22nd international conference mixed design of integrated circuits & systems (MIXDES)*, 2015, pp. 181–186. doi: 10.1109/MIXDES.2015.7208507.

[10] Han, H.-C. and A. D'Amico and C. Enz, "SEKV-E: Parameter Extractor of Simplified EKV I-V model for Low-power Analog Circuits." https://gitlab.com/moscm/sekv-e, 2022.

[11] F. Krummenacher, E. Vittoz, and M. Degrauwe, "Class AB CMOS amplifier micropower SC filters," *Electronics Letters*, vol. 17, no. 13, pp. 433–435, 1981.

[12] M. G. Degrauwe, J. Rijmenants, E. A. Vittoz, and H. J. D. Man, "Adaptive biasing CMOS amplifiers," *IEEE Journal of Solid-State Circuits*, vol. 17, no. 3, pp. 522–528, 1982.

[13] C. C. Enz, F. Krummenacher, and E. A. Vittoz, "An Analytical MOS Transistor Model Valid in All Regions of Operation and Dedicated to Low-Voltage and Low-Current Applications," *Analog Integrated Circuits and Signal Processing Journal*, vol. 8. https://github.com/chrisenz/EKV/tree/main/EKV2.6/docs/EKV_original_paper_1995_prepub.pdf, pp. 83–114, 1995.

[14] Dietmar Warning, "Verilog-A Models for Circuit Simulation." https://github.com/dwarning/VA-Models, 2024.

[15] SemiMod GmbH, "Open VAF." https://openvaf.semimod.de/docs/getting-started/introduction/, 2025.